Available online at www.sciencedirect.com

SciVerse ScienceDirect

Geochimica et Cosmochimica Acta 109 (2013) 280–295

Geochimica et Cosmochimica Acta

www.elsevier.com/locate/gca

Contemporaneous formation of chondrules in distinct oxygen isotope reservoirs

Takayuki Ushikubo [a,*], Daisuke Nakashima [a], Makoto Kimura [b], Travis J. Tenner [a], Noriko T. Kita [a]

[a] WiscSIMS, Department of Geoscience, University of Wisconsin, Madison, WI 53706, USA
[b] Faculty of Science, Ibaraki University, Mito, Ibaraki 310-8512, Japan

Received 5 July 2012; accepted in revised form 15 January 2013; Available online 13 February 2013

Abstract

We investigated the ^{26}Al–^{26}Mg systematics of type I (FeO-poor) chondrules from one of the most primitive carbonaceous chondrites, Acfer 094. The inferred initial $^{26}Al/^{27}Al$ ratios of chondrules from Acfer 094 ranged from $(4.2 \pm 2.0) \times 10^{-6}$ to $(9.0 \pm 1.5) \times 10^{-6}$. These chondrules have distinct oxygen isotope ratios ($\Delta^{17}O$: −5‰, −2‰, and 0‰), though no correlation between inferred initial $^{26}Al/^{27}Al$ ratios and oxygen isotope ratios were observed. These results indicate the regional oxygen isotope heterogeneity in the solar nebula over the duration of chondrule formation.

A few low-Ca pyroxene grains in chondrules have small but resolvable ^{26}Mg excesses at the level of ~0.1‰, which may be the result of a partial melting of chondrules by reheating events. If this is the case, the true inferred initial $^{26}Al/^{27}Al$ ratios of these particular chondrule could be slightly lower (<10%) than estimates using Mg isotope ratios of coexisting plagioclase and olivine.

Stable isotope ratios of Mg ($^{25}Mg/^{24}Mg$) of many olivine grains in chondrules are positively fractionated by ~1‰ relative to those in other phases within the same chondrules. This suggests that olivine preserved a positively fractionated Mg isotope ratios of the chondrule-forming melt prior to significant condensation during the cooling stage of chondrule formation.

1. INTRODUCTION

Chondrules are igneous silicate spherules that formed in the solar nebula. As chondrules are abundant in various types of primitive chondrites, melting of silicate particles by temporal heating was a common phenomenon in the solar nebula (Connolly and Love, 1998). The timing of chondrule formation has been estimated by using the U–Pb absolute chronometer (Amelin et al., 2002, 2010; Connelly et al., 2008) as well as using the decay of the short-lived radionuclide ^{26}Al (half life: 0.705 Ma, Norris et al., 1983) as a relative chronometer. In most chondrules from type 3.0 to 3.1 chondrites, excesses of ^{26}Mg due to the decay of ^{26}Al can be resolved and the inferred initial $^{26}Al/^{27}Al$ ratios, $(^{26}Al/^{27}Al)_0$, have been estimated to be ~$(0.5–1.5) \times 10^{-5}$ (Hutcheon and Hutchison, 1989; Russell et al., 1996; Kita et al., 2000; Huss et al., 2001; Mostefaoui et al., 2002; Yurimoto and Wasson, 2002; Kunihiro et al., 2004; Rudraswami and Goswami, 2007; Kurahashi et al., 2008a; Rudraswami et al., 2008; Hutcheon et al., 2009; Villeneuve et al., 2009). Assuming homogeneous distribution of ^{26}Al in the early Solar System, these initial $^{26}Al/^{27}Al$ ratios correspond to the formation of chondrules 1–3 Ma after Ca, Al-rich inclusions (hereafter CAIs) ($(^{26}Al/^{27}Al)_0$ ~ 5.2×10^{-5}; e.g. Jacobsen et al., 2008; MacPherson et al., 2010, 2012; Larsen et al., 2011). However, ^{26}Mg excesses are limited or not resolved for most chondrules in CR chondrites (Nagashima et al., 2007, 2008; Kurahashi et al., 2008b) as well as a chondrule-like object in the comet Wild 2 (Ogliore et al., 2012) with low inferred initial $^{26}Al/^{27}Al$ ratios ($<3 \times 10^{-6}$), indicating their relatively younger formation ages (>3 Ma after CAIs).

Recently, a bimodal distribution of oxygen isotope ratios in chondrules and their correlation with Mg# (Molar

* Corresponding author.
E-mail address: ushi@geology.wisc.edu (T. Ushikubo).

0016-7037/$ - see front matter © 2013 Elsevier Ltd. All rights reserved.
http://dx.doi.org/10.1016/j.gca.2013.01.045

[MgO]/[MgO + FeO] % of constituent olivine and/or low-Ca pyroxene) were recognized from the Acfer 094 ungrouped carbonaceous chondrite (Ushikubo et al., 2012). Many FeO-poor chondrules (Mg#⩾98) have $\Delta^{17}O$ values (=$\delta^{17}O$–0.52 × $\delta^{18}O$) of ∼ −5‰, while chondrules with Mg#'s of 95-40 have higher $\Delta^{17}O$ values of ∼ −2‰, with a few exceptions having $\Delta^{17}O$ values of ∼0 and −9‰. A similar correlation between oxygen isotope ratios and Mg# has been recognized among chondrules from other carbonaceous chondrites (Wasson et al., 2004; Connolly and Huss, 2010; Nakashima et al., 2010; Rudraswami et al., 2011; Tenner et al., 2012, 2013; Schrader et al., 2013). As chondrules with higher $\Delta^{17}O$ values are comparably FeO-rich (low Mg#), this increase in the $\Delta^{17}O$ values of chondrules is closely related to an increase in the oxygen fugacity of the chondrule forming environment, which can be caused by either addition of an oxidizing agent (e.g. H_2O) or enhancement of dust enrichment (Fedkin and Grossman, 2006; Connolly and Huss, 2010; Tenner et al., 2012, 2013; Ushikubo et al., 2012; Schrader et al., 2013). The oxygen isotope ratios and redox states of chondrule forming environments could change with time during the evolution of the early solar nebula, which may be tested by comparing the inferred initial $^{26}Al/^{27}Al$ ratios of chondrules with their $\Delta^{17}O$ values.

In this study, we measured the ^{26}Al–^{26}Mg systematics of type I chondrules (Mg#>90) containing anorthite from Acfer 094, with previously characterized oxygen isotope ratios (Ushikubo et al., 2012), to test the correlation between forming ages of chondrules and their $\Delta^{17}O$ values. The chronological information for chondrules with distinct $\Delta^{17}O$ values provides a temporal constraint on the oxygen isotope ratios of the chondrule-forming environment in the solar nebula. The chondrules of interest have three distinct oxygen isotope components ($\Delta^{17}O$ ∼ −5‰, −2‰, and 0‰) as well as two porphyritic chondrules with highly heterogeneous oxygen isotope ratios. Since Acfer 094 is one of the least metamorphosed carbonaceous chondrites (type 3.00; Grossman and Brearley, 2005; Kimura et al., 2008) and is free from hydrated minerals (Greshake, 1997), chondrules from Acfer 094 are the best samples in which to examine their primary ^{26}Al–^{26}Mg systematics, negating issues due to isotopic disturbance during metamorphism in their parent body (Huss et al., 2001).

2. SAMPLES

We selected 16 FeO-poor type I chondrules from the polished thin section of Acfer 094 (USNM 7233-8), which was provided by the Smithsonian National Museum of Natural History (Table 1). They consist of one Al-rich chondrule and one barred olivine chondrule, while the rest are porphyritic in texture. Three porphyritic chondrules contain refractory forsterite grains which are enriched in elements such as Al and Ca (CaO > 0.5 wt%; Steele, 1986), hereby denoted as "RF-type I" chondrules. Among the collective group of chondrules, ten (one Al-rich and nine type I) have anorthitic plagioclase grains with sizes larger than 5 μm (Fig. 1 and Fig. S2 in electronic annex), and were thus suitable for determination of their initial

Table 1
Petrologic types and elemental compositions of chondrules from Acfer 094 (USNM 7233-8).

Sample name	Type	Texture	Mg#[a,b]	$\Delta^{17}O$[a]	Relict olivine[a,c]	Plagioclase[d]	An[e]
Al-rich							
G15	Al-rich	Porphyritic	99.1	−4.64 ± 0.42		+	96.4
RF-bearing type I							
G56	RF-IAB	Porphyritic	99.5	−5.55 ± 0.37			
G100	RF-IA	Porphyritic	99.5	Heterogeneous[f]	+		
G113	RF-I	Fragment	99.5	−6.27 ± 0.27			
Type I (Mg#⩾97)							
G18	IAB	Porphyritic	98.3	−5.33 ± 0.65		+	95.0
G42	IAB	Porphyritic	98.4	−5.47 ± 0.47			95.9
G46	IAB	Porphyritic	98.9	−4.88 ± 0.29	+	+	98.2
G48	I	Barred ol	99.4	−5.28 ± 0.49			
G68	IAB	Porphyritic	98.0	Heterogeneous[f]	+	+	98.3
G73	IAB	Porphyritic	99.1	−6.16 ± 0.24		+	94.0
G76	IAB	Porphyritic	98.5	−5.08 ± 0.78		+	91.4
G95	IAB	Porphyritic	98.7	−4.77 ± 0.26		+	99.3
Type I (90⩽Mg#<97)							
G45	IAB	Porphyritic	95.2	−2.42 ± 0.36	+	+	94.4
G52	IA	Porphyritic	94.6	−2.19 ± 0.51	+		
G74	IAB	Porphyritic	94.5	−1.93 ± 0.25	+	+	99.1
G39	I	Fragment	92.3	−0.51 ± 0.37		+	95.2

[a] Data from Ushikubo et al. (2012). Errors are 95% confidence level.
[b] Average Mg# value of olivine and low-Ca pyroxene.
[c] + Indicates presence of relict olivine grain(s) identified based on their oxygen isotope compositions.
[d] + Indicates presence of Mg isotope data of plagioclase for the Al–Mg systematics.
[e] Typical An content (molar 100 × [CaO/(CaO + 0.5Na_2O + 0.5K_2O)]) of plagioclase.
[f] Unable to determine average $\Delta^{17}O$ values because of abundant relict olivines.

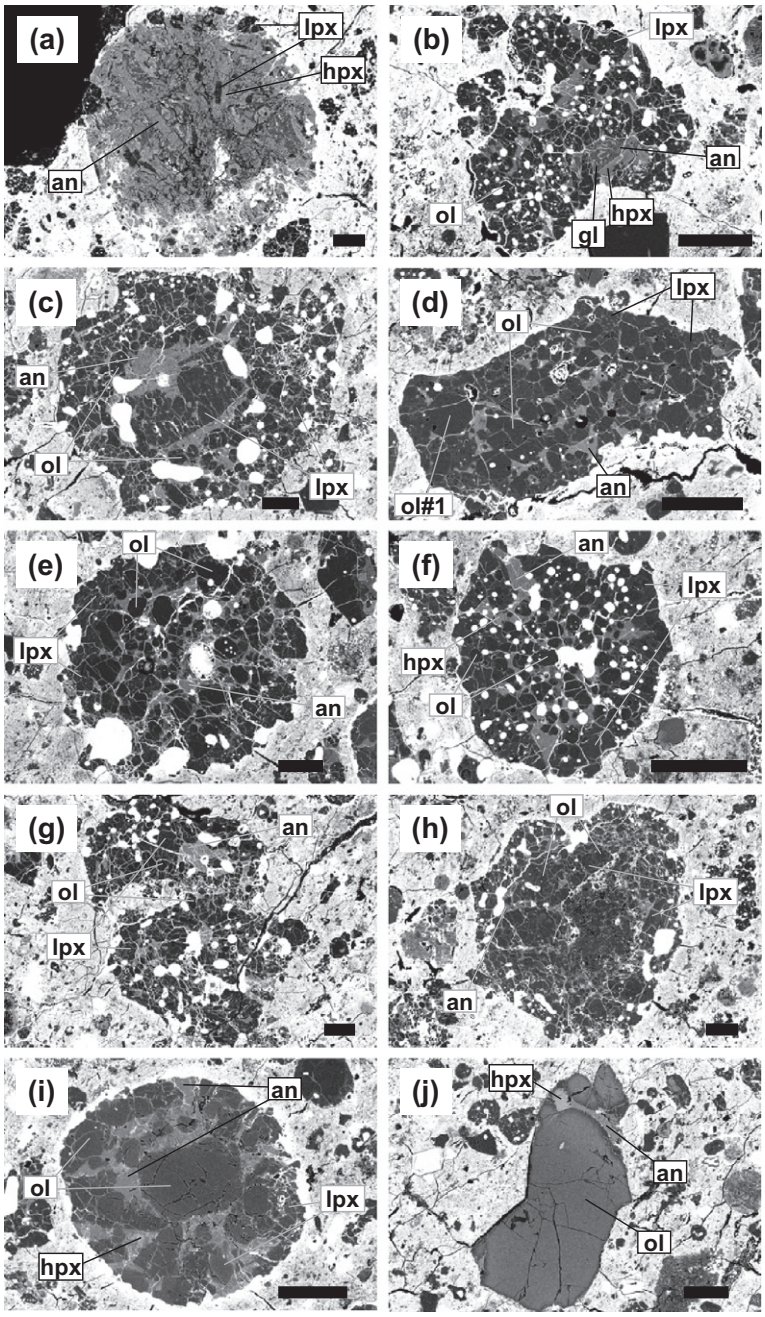

Fig. 1. Backscattered electron (BSE) images of chondrules that were measured to determined initial $^{26}Al/^{27}Al$ ratios. (a) G15 Al-rich, (b) G18 type IAB, (c) G46 type IAB, (d) G68 type IAB with a highly heterogeneous oxygen isotope ratio, (e) G73 type IAB, (f) G76 type IAB, (g) G95 type IAB, (h) G45 type IAB, (i) G74 type IAB, (j) G39 type I fragment. Abbreviations are ol = olivine, lpx = low-Ca pyroxene, hpx = high-Ca pyroxene, an = anorthite, gl = glass. The label of ol#1 in (d) indicates the ^{16}O-rich olivine grain in which we performed the Mg isotope analysis spot #1 (Fig. 3b, Table 2). Scale bars are 100 μm.

$^{26}Al/^{27}Al$ ratios by analysis of olivine, pyroxene and plagioclase to establish an internal isochron. For the remaining 6 chondrules (3 RF-type I and 3 type I, including one barred olivine (BO) chondrule, Fig. 2), Mg isotope ratios were only determined from olivine and pyroxene. Overall, type I chondrules were specifically chosen for analysis because they contain anorthitic plagioclase in their mesostasis, whereas type II chondrules typically contain albitic plagioclase (e.g., Kurahashi et al., 2008a). This constraint was placed upon the selection of chondrules because it has been recently demonstrated that the Mg diffusion rate in albitic plagioclase is significantly faster than anorthitic plagioclase (e.g., Mg isotopic diffusion of oligoclase (An_{23}) is more than two orders of magnitude faster than in anorthite (An_{93}), Van Orman et al., 2012), and therefore ^{26}Al–^{26}Mg systematics of albite-bearing type II chondrules are susceptible to

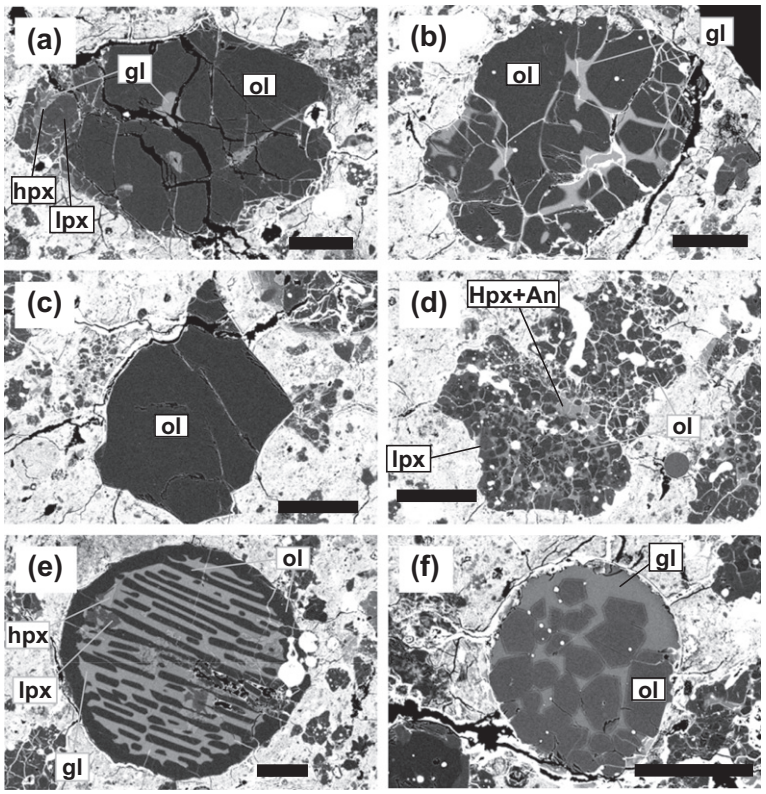

Fig. 2. BSE images of chondrules that were measured to quantify the Mg isotope ratios of ferromagnesian minerals. (a) G56 RF-type IAB, (b) G100 RF-type IA, (c) G113 RF type I fragment, (d) G42 type IAB, (e) G48 type I barred olivine, (f) G52 type IA. Scale bars are 100 μm.

disturbance that likely affect their isochron determinations. Although type II chondrules were excluded, the oxygen isotopic compositions of the type I samples cover the range of type II chondrules ($\Delta^{17}O \sim -2‰$ and 0‰) in Acfer 094 (Table 1 and Figs. 3 and 4).

G15 (Fig. 1a) is an Al-rich chondrule, consisting of anorthitic plagioclase, low-Ca pyroxene, high-Ca pyroxene, and glass. The composition of pyroxene is Mg-rich (Mg# of low-Ca pyroxene: 99.1). The $\Delta^{17}O$ value of G15 is $\sim -4.6‰$ (Fig. 4). G56 (Fig. 2a), G100 (Fig. 2b), and G113 (Fig. 2c) are RF-type I chondrules (G113 is a chondrule fragment) that contain refractory forsterite (Mg#∼99.5, CaO ∼ 0.5 to 0.7 wt%) with bright blue cathodoluminescence (Ushikubo et al., 2012). Other phases in these RF-type I chondrules include low-Ca pyroxene, high-Ca pyroxene, and glass. The $\Delta^{17}O$ values of G56 and G113 are $\sim -5.6‰$ and $\sim -6.3‰$ (Fig. 4), respectively. The oxygen isotope ratios of G100 are heterogeneous but the range of the observed oxygen isotope ratios are relatively narrow ($\Delta^{17}O = -6.7‰$ to $-2.4‰$; Ushikubo et al., 2012).

The remaining 12 type I chondrules can be divided into three subgroups based on their Mg# and the $\Delta^{17}O$ values. Eight chondrules (G18, 42, 46, 48, 68, 73, 76, and 85) consist mainly of highly magnesian (Mg# = 98.0 to 99.4) olivine and low-Ca pyroxene. They exhibit porphyritic textures with plagioclase and/or glass in the mesostasis, except for BO chondrule G48 (Fig. 2e) that consists of olivine, low-Ca pyroxene, high-Ca pyroxene, and glass. Their $\Delta^{17}O$ values, excluding G68, range from $-6.2‰$ to $-4.8‰$ (Fig. 4). G68 (Fig 1d) is an irregular shaped type I chondrule and has a highly heterogeneous oxygen isotopic composition containing ^{16}O-rich relict olivine grains (down to $-23‰$ in $\Delta^{17}O$, $-43‰$ in $\delta^{18}O$, Fig. 3b). Three chondrules (G45, 52, and 74, Figs. 1h,i, 2f, respectively) consist of olivine and low-Ca pyroxene phenocrysts with Mg#∼95 and their $\Delta^{17}O$ values range from $-2.4‰$ to $-1.9‰$ (Fig. 4). G39 (Fig. 1j) is an olivine fragment with small amounts of high-Ca pyroxene and plagioclase. The oxygen isotope ratio of a chondrule fragment G39 (Mg#∼92) is ^{16}O-poor ($\sim -0.5‰$ in $\Delta^{17}O$, Fig. 4) relative to other chondrules from Acfer 094. The Mg# of olivine cores in G39 is 92.3, but they exhibit reverse zoning at the edge to Mg#∼96.

3. ANALYTICAL PROCEDURES

3.1. Electron microscopy

For petrographic observation of chondrules, backscattered electron (BSE), secondary electron (SE), and cathodoluminescence images were obtained by a Hitachi S-3400N Scanning electron microscope (SEM) at University of Wisconsin-Madison (UW-Madison). Major element compositions in minerals and glass were obtained using the JEOL 733 electron-probe microanalyzer (EPMA) at Ibaraki University. The analytical conditions and results are reported in Ushikubo et al. (2012). The bulk compositions of chondrules were measured with broad beam EPMA, and corrected by the method after Ikeda (1980). Although the

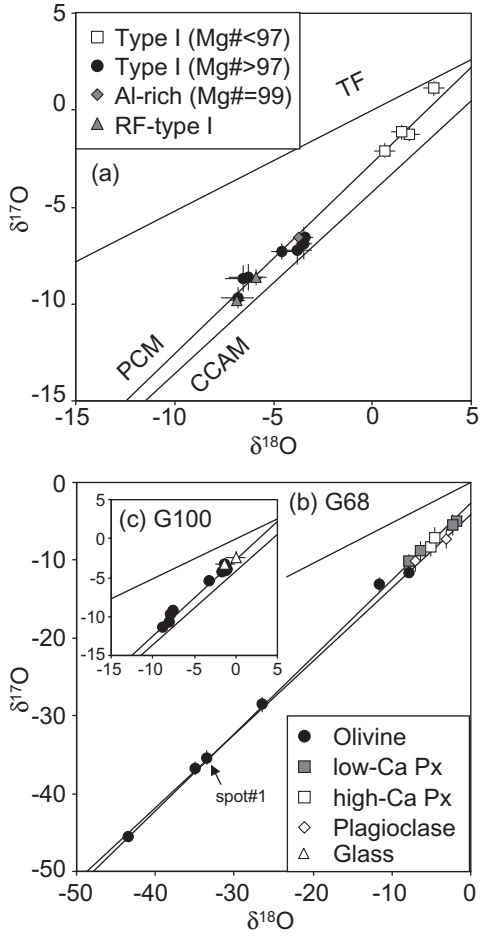

Fig. 3. Oxygen three isotope plot of (a) the average values of the chondrules included in this study, and individual oxygen isotope data of (b) G68 and (c) G100, which exhibit heterogeneous oxygen isotopic compositions (data from Ushikubo et al., 2012). The oxygen isotope data labeled as spot #1 in (b) is the data of the olivine grain which we measured Mg isotope data (spot #1 of G68 in Table 2).

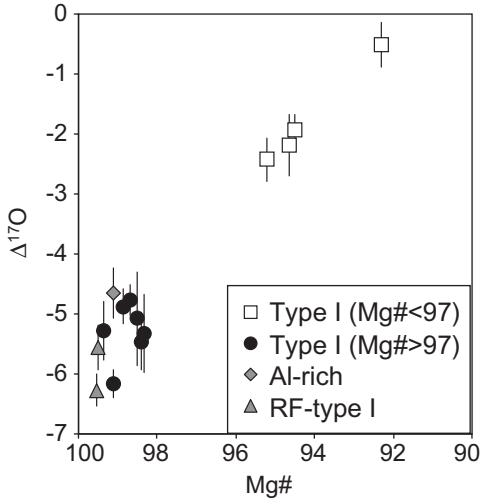

Fig. 4. $\Delta^{17}O$–Mg# diagram of chondrules in this study (data are from Ushikubo et al., 2012). Two chondrules that have heterogeneous oxygen isotope ratios are not shown. Errors for $\Delta^{17}O$ are 95% confidence.

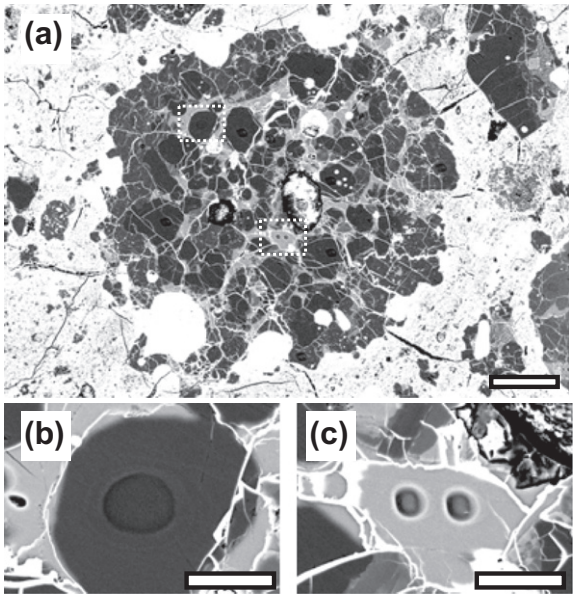

Fig. 5. An example of analysis pits. (a) BSE image of the chondrule G73. Regions outlined by dotted-dash lines are shown in detail in (b) and (c). (b) BSE image of Mg isotope analysis pit of olivine with a 15 μm beam. (c) BSE image of Mg isotope analysis pit of plagioclase with a 5 μm beam. Scale bars are 100 μm for (a) and 20 μm for (b) and (c).

quality of broad beam EPMA analysis is not as good as spot EPMA analysis due to the lack of capability of a matrix correction (e.g., metal, glass, and ferromagnesian silicates), this technique is still useful to determine the Al/Mg ratios of bulk chondrules. Higher totals are due to tiny metal and troilite grains, which could not be avoided during broad beam analysis. However, the Al/Mg ratios are not influenced by such contamination. Estimated bulk compositions of chondrules are summarized in Table S1 in electronic annex.

3.2. Magnesium isotope analysis by secondary ion mass spectrometry

Magnesium three-isotopes and Al/Mg ratios of minerals in chondrules were analyzed using the CAMECA IMS-1280 Secondary Ion Mass Spectrometer (SIMS) at UW-Madison (WiscSIMS). The analytical conditions are generally similar to those of Kita et al. (2012). Primary O^- ions were used to sputter the sample to extract secondary ions of Mg^+ and Al^+, by applying primary and secondary acceleration voltages of −13 and +10 kV, respectively. Secondary ion optics were adjusted by using ×200 magnification for the transfer lens setting and circular mode for coupling lens settings. The entrance slit width was set to ~90 μm. Other parameters were adjusted according to two different analytical conditions that were applied to mafic minerals (olivine and pyroxene) and plagioclase, due to the difference in their secondary Mg^+ ion intensities.

Table 2
Al–Mg systematics of ten chondrules from Acfer 094 (USNM-7233-8).

Sample name	Spot # phase	$^{27}Al/^{24}Mg$ (2 SE)	$\delta^{26}Mg^*$ (2 SE)	$\delta^{25}Mg$ (2 SE)
Al-rich				
G15	1 LPx	0.04 ± 0.01	0.07 ± 0.08	1.32 ± 0.29
(Al-rich)	2 Pl	34.58 ± 0.50	1.26 ± 0.89	−−[a]
	3 Pl	33.68 ± 0.48	1.03 ± 0.77	1.54 ± 0.55
	4 Pl	33.78 ± 0.49	2.00 ± 0.99	1.03 ± 0.66
	5 Pl	32.82 ± 0.47	1.92 ± 0.77	0.86 ± 0.62
		$(^{26}Al/^{27}Al)_0 = (6.0 \pm 1.7) \times 10^{-6}$	$\delta^{26}Mg^*_0 = 0.07 \pm 0.08$	
Type I (Mg# ⩾ 97)				
G18	1 LPx	0.03 ± 0.01	-0.01 ± 0.08	0.36 ± 0.29
(Type IAB)	2 LPx	0.04 ± 0.01	0.00 ± 0.08	0.21 ± 0.29
	3 HPx	0.10 ± 0.01	0.03 ± 0.08	0.56 ± 0.29
	4 Pl	36.89 ± 0.53	1.81 ± 0.94	0.0 ± 0.54
	5 Pl	32.33 ± 0.54	0.32 ± 1.03	−−[a]
		$(^{26}Al/^{27}Al)_0 = (4.7 \pm 2.8) \times 10^{-6}$	$\delta^{26}Mg^*_0 = 0.00 \pm 0.04$	
G46	1 Ol	<0.01	0.00 ± 0.05	1.72 ± 0.16
(Type IAB)	2 Ol	<0.01	0.03 ± 0.04	1.77 ± 0.16
	3 LPx	0.02 ± 0.01	-0.03 ± 0.05	0.53 ± 0.16
	4 Pl	26.91 ± 0.39	1.15 ± 0.90	0.40 ± 0.55
	5 Pl	28.68 ± 0.42	0.96 ± 0.99	0.45 ± 0.54
	6 Pl	28.47 ± 0.41	0.78 ± 0.90	0.55 ± 0.52
		$(^{26}Al/^{27}Al)_0 = (4.7 \pm 2.7) \times 10^{-6}$	$\delta^{26}Mg^*_0 = 0.00 \pm 0.03$	
G68	1 Ol	<0.01	0.01 ± 0.04	1.87 ± 0.16
(Type IAB)	2 Ol	<0.01	0.01 ± 0.04	1.90 ± 0.16
	3 LPx	0.03 ± 0.01	0.01 ± 0.05	0.18 ± 0.16
	4 Pl	39.50 ± 0.57	2.09 ± 1.00	0.20 ± 0.57
	5 Pl	44.82 ± 0.64	1.12 ± 0.92	0.39 ± 0.51
		$(^{26}Al/^{27}Al)_0 = (5.0 \pm 2.2) \times 10^{-6}$	$\delta^{26}Mg^*_0 = 0.01 \pm 0.02$	
G73	1 Ol	<0.01	-0.01 ± 0.05	1.32 ± 0.16
(Type IAB)	2 Ol	<0.01	-0.01 ± 0.04	1.28 ± 0.16
	3 LPx	0.04 ± 0.01	-0.01 ± 0.06	0.61 ± 0.16
	4 Pl	41.77 ± 0.61	2.14 ± 0.90	0.12 ± 0.55
	5 Pl	46.80 ± 0.68	2.39 ± 0.95	0.43 ± 0.55
	6 Pl	40.12 ± 0.60	2.52 ± 1.00	0.04 ± 0.57
		$(^{26}Al/^{27}Al)_0 = (7.6 \pm 1.8) \times 10^{-6}$	$\delta^{26}Mg^*_0 = -0.01 \pm 0.03$	
G76	1 Ol	<0.01	0.03 ± 0.05	2.29 ± 0.18
(Type IAB)	2 LPx	0.03 ± 0.01	-0.03 ± 0.05	0.68 ± 0.18
	3 LPx	0.02 ± 0.01	0.03 ± 0.04	0.49 ± 0.18
	4 Pl	27.98 ± 0.41	0.98 ± 0.87	−−[b]
	5 Pl	*34.53* ± 0.64	*1.64* ± 1.73	0.48 ± 0.85
	6 Pl	33.61 ± 0.48	1.20 ± 0.94	0.50 ± 0.55
		$(^{26}Al/^{27}Al)_0 = (5.1 \pm 2.7) \times 10^{-6}$	$\delta^{26}Mg^*_0 = 0.01 \pm 0.03$	
G95	1 Ol	<0.01	0.02 ± 0.04	1.60 ± 0.18
(Type IAB)	2 LPx	0.03 ± 0.01	0.01 ± 0.05	0.45 ± 0.18
	3 LPx	0.03 ± 0.01	0.04 ± 0.05	0.43 ± 0.18
	4 Pl	51.99 ± 0.75	1.56 ± 1.02	0.02 ± 0.58
	5 Pl	51.44 ± 0.74	1.93 ± 0.98	0.18 ± 0.53
	6 Pl	54.50 ± 0.78	2.08 ± 1.05	-0.04 ± 0.56
		$(^{26}Al/^{27}Al)_0 = (4.9 \pm 1.5) \times 10^{-6}$	$\delta^{26}Mg^*_0 = 0.02 \pm 0.03$	
Type I (90 ⩽ Mg# < 97)				
G45	1 Ol	<0.01	0.05 ± 0.04	1.70 ± 0.13
(Type IAB)	2 LPx[b]	0.06 ± 0.01	0.13 ± 0.04	0.95 ± 0.13
	3 LPx	0.05 ± 0.01	0.02 ± 0.05	0.80 ± 0.13
	4 Pl	47.56 ± 0.69	2.09 ± 1.15	0.65 ± 0.90
	5 Pl	48.47 ± 0.70	0.91 ± 1.14	0.99 ± 0.59
	6 Pl	43.67 ± 0.63	1.41 ± 1.11	0.16 ± 0.64
		$(^{26}Al/^{27}Al)_0 = (4.2 \pm 2.0) \times 10^{-6}$	$\delta^{26}Mg^*_0 = 0.04 \pm 0.03$	

Table 2 *(continued)*

Sample name	Spot # phase	$^{27}Al/^{24}Mg$ (2 SE)	$\delta^{26}Mg^*$ (2 SE)	$\delta^{25}Mg$ (2 SE)
G74	1 Ol	<0.01	0.00 ± 0.04	1.60 ± 0.18
(Type IAB)	2 Ol	<0.01	0.06 ± 0.04	1.64 ± 0.18
	3 LPx[b]	0.11 ± 0.01	0.13 ± 0.06	1.44 ± 0.18
	4 Pl	32.81 ± 0.47	1.48 ± 0.82	0.33 ± 0.52
	5 Pl	36.32 ± 0.52	1.12 ± 0.80	0.60 ± 0.50
	6 Pl	32.09 ± 0.47	1.66 ± 0.83	0.15 ± 0.53
		$(^{26}Al/^{27}Al)_0 = (5.6 \pm 2.0) \times 10^{-6}$	$\delta^{26}Mg^*_0 = 0.03 \pm 0.03$	
G39	1 Ol	<0.01	0.03 ± 0.06	0.65 ± 0.13
(Type I)	2 Ol	<0.01	0.00 ± 0.04	0.68 ± 0.13
	3 Pl	44.74 ± 0.65	2.74 ± 0.82	-0.72 ± 0.53
	4 Pl	48.85 ± 0.70	3.32 ± 0.91	-0.65 ± 0.55
	5 Pl	44.31 ± 0.64	2.95 ± 1.01	-0.37 ± 0.64
		$(^{26}Al/^{27}Al)_0 = (9.0 \pm 1.5) \times 10^{-6}$	$\delta^{26}Mg^*_0 = 0.01 \pm 0.03$	

[a] $\delta^{25}Mg$ data are omitted because the analysis pit overlap with the previous oxygen isotope analysis pit.
[b] $\delta^{26}Mg^*$ data was not used to calculate the isochron. See the Section 5.2.2.

3.2.1. Multi-Faraday cup analyses of olivine and pyroxene

Magnesium three-isotopes and Al/Mg ratios for olivine and pyroxene were measured using a primary O^- beam that was ~15 μm in diameter and ~4.5 nA in intensity (Fig. 5b). The field aperture was set to 5000 μm square, corresponding to a ~25 μm square field of view on a sample. Secondary ions ($^{24}Mg^+$, $^{25}Mg^+$, $^{26}Mg^+$, and $^{27}Al^+$) were detected by multiple Faraday cup (FC) detectors, simultaneously, with an exit slit width of 500 μm. Mass resolving power (M/ΔM) at 10% height was ~2500 and the tailing of interference peaks, such as $^{48}Ca^{2+}$ and MgH^+ were negligibly small at the center of the Mg^+ mass spectrum (less than 0.01‰). The measured Mg isotope ratios ($^{25}Mg/^{24}Mg$ and $^{26}Mg/^{24}Mg$) are converted to the δ-notation ($\delta^{25}Mg_{raw}$ and $\delta^{26}Mg_{raw}$ values) by normalizing to the terrestrial reference ratios of $(^{25}Mg/^{24}Mg) = 0.12663$ and $(^{26}Mg/^{24}Mg) = 0.13932$ (Catanzaro et al., 1966), respectively. The relative sensitivity factor ($RSF = (^{27}Al^+/^{24}Mg^+)/(^{27}Al/^{24}Mg)$) for pyroxene was 0.83 ± 0.05.

The instrumental bias for olivine and pyroxene analyses were determined by using four olivine and three pyroxene standards, which are also used as oxygen isotope standards (Table EA3-2 in Kita et al., 2010). They include San Carlos olivine (SCol, Fo_{89}), which was used as a running standard, one synthetic forsterite standard NH-Ol (Fo_{100}), and two natural olivine standards, IG-Ol (Fo_{90}) and OR-Ol (Fo_{60}), two natural orthopyroxene standards, SP79-11 (En_{97}) and JE-En (En_{85}), and one diopside standard, 95AK-6 ($En_{47}Wo_{51}$). It is assumed that the Mg isotopes in these standards are the same as the literature data of global peridotite xenoliths ($\delta^{25}Mg = -0.13 \pm 0.03$‰ in DSM3 scale; Teng et al., 2010). This assumption may be valid for natural mineral standards at the level of ±0.3‰ (Handler et al., 2009; Shen et al., 2009). Details for the instrumental bias correction are described in electronic annex.

The ^{26}Mg-excess after mass fractionation correction ($\delta^{26}Mg^*$) is calculated using an exponential law of $\delta^{26}Mg^* = \delta^{26}Mg - (1 + \delta^{25}Mg/1000)^{-0.514}$ (Davis et al., 2005). A positive offset of $\delta^{26}Mg^*_{raw}$ ($=\delta^{26}Mg_{raw} - (1 + \delta^{25}Mg_{raw}/1000)^{-0.514}$) values of $\sim 0.2 \pm 0.1$‰ were consistently obtained by analyses of standards and there was no correlation with compositions of standard minerals (electronic annex). Because this offset is likely caused by the difference in the efficiency of three FC detectors for $^{24}Mg^+$, $^{25}Mg^+$, and $^{26}Mg^+$, respectively, we calculated the average offset value of bracketing analyses of San Carlos olivine ($\delta^{26}Mg^*_{raw}$(SCol)) and the $\delta^{26}Mg^*$ values of samples were calculated by $\delta^{26}Mg^*(sample) = \delta^{26}Mg^*_{raw}(sample) - \delta^{26}Mg^*_{raw}(SCol)$.

Uncertainties of $\delta^{25}Mg$ and $\delta^{26}Mg^*$ values of samples are assigned to be the same as the spot-to-spot reproducibility (2SD, 2 standard deviation) of the San Carlos olivine bracketing analyses. Typical uncertainties (2SD) of bracketing San Carlos olivine analyses are ±0.18‰ and ±0.05‰ for $\delta^{25}Mg$ and $\delta^{26}Mg^*$ values, respectively. As a result of the lower count rates of Mg ions of pyroxene relative to those of San Carlos olivine, uncertainties of Mg isotope analysis of pyroxene can be larger than those of San Carlos olivine. When uncertainties calculated by both the internal error of an individual sample analysis ($2SE_{internal}$, 2 standard error of the mean of 30 cycles in a single analysis) and the 2 SE of bracketing San Carlos olivine analyses ($2SE_{std}$) are larger than the spot-to-spot reproducibility (2 SD) of the bracketing San Carlos olivine analyses, we assign the value of $\{(2SE_{internal})^2 + (2SE_{std})^2\}^{1/2}$ as the uncertainties of the sample data (electronic annex).

After the analytical session, SIMS pit conditions were assessed by SEM and data from pits with irregularities (e.g. existence of cracks or inclusions) were rejected.

3.2.2. Magnesium isotope analysis for plagioclase

Magnesium three-isotopes and Al/Mg ratios for plagioclase were measured by a 13 kV accelerated lower intensity primary O^- beam (~70 pA) of ~5 μm in diameter (Fig. 5c). Secondary ion optics were adjusted to ×200 magnification from the sample to the field aperture (4000 μm square) resulting in a 20 μm square field of view. The mass resolving power (M/ΔM) was set at ~4000, which is suitable for the separation of $^{48}Ca^{2+}$ and MgH^+ interferences from the Mg^+ mass spectrum. Secondary Mg^+ ions were detected by an axial electron multiplier (EM) that operated by magnetic peak switching. During the measurement of $^{25}Mg^+$,

Table 3
Mg isotope ratios of other six chondrules from Acfer 094 (USNM-7233-8).

Sample name	Spot # phase	$^{27}Al/^{24}Mg$ (2 SE)	$\delta^{26}Mg^*$ (2 SE)	$\delta^{25}Mg$ (2 SE)
RF-bearing type I				
G56	1 Ol	<0.01	0.00 ± 0.04	0.45 ± 0.13
(RF-type IAB)	2 Ol	<0.01	−0.01 ± 0.05	0.92 ± 0.13
Average			0.00 ± 0.03	
G100	1 Ol	<0.01	−0.03 ± 0.04	0.43 ± 0.13
(RF-type IA)	2 Ol	<0.01	0.01 ± 0.04	0.74 ± 0.13
Average			−0.01 ± 0.03	
G113	1 Ol	<0.01	0.00 ± 0.04	0.62 ± 0.13
(RF-type I)				
Type I (Mg# ⩾ 97)				
G42	1 Ol	<0.01	0.02 ± 0.05	1.87 ± 0.13
(Type IAB)	2 LPx	0.02 ± 0.01	0.03 ± 0.05	0.22 ± 0.13
Average			0.03 ± 0.03	
G48	1 Ol	<0.01	0.05 ± 0.04	1.20 ± 0.13
(Type I BO)	2 Ol	<0.01	0.04 ± 0.05	1.27 ± 0.13
Average			0.05 ± 0.03	
Type I (90 ⩽ Mg# < 97)				
G52	1 Ol	<0.01	0.01 ± 0.05	1.74 ± 0.13
(Type IA)	2 Ol	<0.01	0.01 ± 0.05	1.77 ± 0.13
Average			0.01 ± 0.04	

secondary $^{27}Al^+$ ions were simultaneously detected by a FC on an additional trolley, located on the high mass side of the axial EM (Kita et al., 2012). Dead time of the EM determined by Mg isotope data of anorthitic glasses was 25.4 ± 2.3 ns. Counting times of individual ions for each cycle were 3s for $^{24}Mg^+$ and 10s for $^{25}Mg^+$, $^{26}Mg^+$, and $^{27}Al^+$, respectively. The total number of cycles for each Mg isotope analysis was 300.

The data reduction procedure of Mg isotope ratios ($^{25}Mg/^{24}Mg$ and $^{26}Mg/^{24}Mg$) is similar to those for olivine and pyroxene (see Section 3.1). Because all Mg ions were measured by an axial EM detector, no offset correction for the $\delta^{26}Mg^*$ value is applied.

Magnesium isotope ratios and $^{27}Al/^{24}Mg$ ratios of three anorthitic synthetic glasses, each with a $\delta^{25}Mg$ value of −1.77‰ on the DSM3 scale (1 wt% MgO, 0.6 wt% MgO, and 0.1 wt% MgO, respectively; Kita et al., 2012), were measured to determine the correction factor for anorthite ($\alpha_{anorthite}$) and the RSF ($(^{27}Al^+/^{24}Mg^+)/(^{27}Al/^{24}Mg) = 1.019 \pm 0.014$). The synthetic anorthitic glass containing 1 wt% MgO was used as a running standard, and the $\delta^{25}Mg$ spot-to-spot analytical uncertainty was ±0.21‰ ($2SE_{std}$, $n = 13$). Uncertainties of the measurements of unknowns are assigned as $\{(2SE_{internal})^2 + (2SE_{std})^2\}^{1/2}$ for $\delta^{25}Mg$ and $2SE_{internal}$ for $\delta^{26}Mg^*$, respectively (electronic annex).

After the analytical session, SEM imaging of the SIMS pits revealed that some of the Mg isotope analyses (~5 μm in diameter) overlapped with SIMS pits from oxygen isotope analyses (~2 μm in diameter by a Cs^+ primary beam). In such cases, $\delta^{26}Mg^*$ values were accepted in order to discuss initial ^{26}Al abundances, but we did not use corresponding $\delta^{25}Mg$ values to discuss mass-dependent Mg isotope fractionation because irregular shapes at the bottom of analysis pits might cause unexpected mass-dependent fractionation (Table 2).

4. RESULTS

4.1. The ^{26}Al–^{26}Mg systematics and $\delta^{26}Mg^*$ values of olivine and pyroxene

Magnesium isotope data of chondrules are summarized in Table 2 and Table 3. Backscattered electron (BSE) images and analysis positions of samples are summarized in Fig. S2 in electronic annex. Of the ten chondrules with sufficient plagioclase, the $^{27}Al/^{24}Mg$ ratios range from 27 to 55 and have significant ^{26}Mg-excesses (positive $\delta^{26}Mg^*$ values) of up to 3.3‰, indicating the existence of extinct ^{26}Al when plagioclase crystallized. The ^{26}Al–^{26}Mg systematics of individual chondrules is shown in Fig. 6. To calculate isochrons of chondrules, we used two or more Mg isotope data from both ferromagnesian minerals (olivine and pyroxene phenocrysts) and plagioclase in each chondrule, respectively. We excluded two outlier pyroxene data (one from G45 and one from G74, Table 2), which exhibit positive $\delta^{26}Mg^*$ values (~0.13‰) and are distinct from $\delta^{26}Mg^*$ values of other olivine and pyroxene phenocrysts in the same chondrule. In addition, relict olivine grains with distinct oxygen isotope ratios might have distinct Mg isotope ratios as well, due to different origins and lack of isotopic exchange. The possibility of isotope heterogeneity in chondrules is assessed in Section 5.2.2.

The inferred initial $^{26}Al/^{27}Al$ ratios, $(^{26}Al/^{27}Al)_0$, of chondrules range from $(4.2 \pm 2.0) \times 10^{-6}$ to $(9.0 \pm 1.5) \times 10^{-6}$ (Fig. 6 and Table 2). Chondrule G39 has a high $(^{26}Al/^{27}Al)_0$ of $(9.0 \pm 1.5) \times 10^{-6}$, which marginally overlaps with the $(^{26}Al/^{27}Al)_0$ values of other chondrules. Nine of ten chondrules have consistent $(^{26}Al/^{27}Al)_0$ values within analytical uncertainties although G73 chondrule has slightly higher $(^{26}Al/^{27}Al)_0$ values. The weighted average in $(^{26}Al/^{27}Al)_0$ values of the nine internally consistent

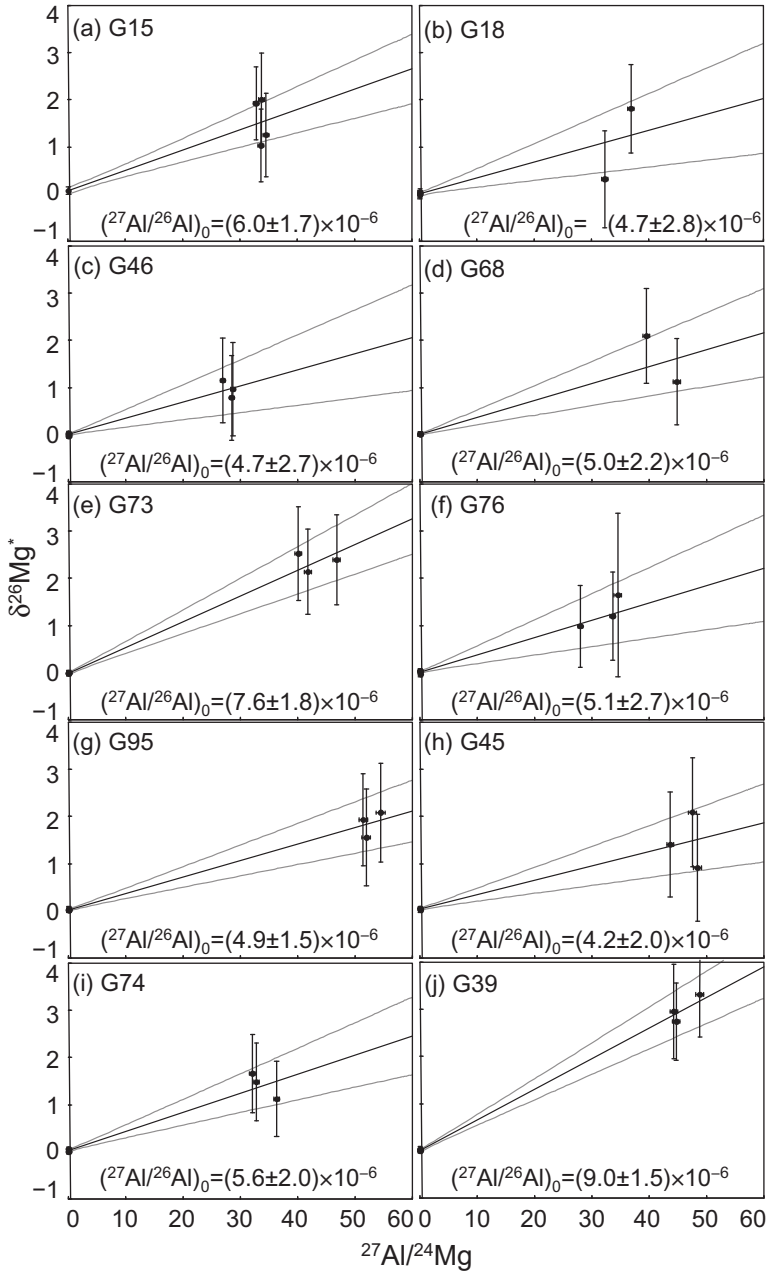

Fig. 6. Al–Mg isochron diagrams of the ten chondrules shown in Fig. 1. Errors are 95% confidence.

chondrules is $(5.4 \pm 0.7) \times 10^{-6}$. Fig. 7 shows the relationship between $(^{26}Al/^{27}Al)_0$ and oxygen isotopic compositions ($\Delta^{17}O$). Although two chondrules with $\Delta^{17}O$ values of $-0.5‰$ and $-6.3‰$ exhibit higher $(^{26}Al/^{27}Al)_0$ values, there is no clear correlation between $(^{26}Al/^{27}Al)_0$ and oxygen isotopic compositions among chondrules from Acfer 094. It is worth mentioning that the $(^{26}Al/^{27}Al)_0$ of G68, which contains highly heterogeneous oxygen isotope ratios (Fig. 3b), is also consistent with other Acfer 094 chondrules which have homogeneous oxygen isotope ratios (Fig. 7).

The $\delta^{26}Mg^*_0$ values as intercepts of internal isochrons from ten chondrules as well as the average $\delta^{26}Mg^*$ values from the 6 chondrules where only the Mg isotope ratios of olivine and low-Ca pyroxene phenocrysts were measured, are shown in Fig. 8. As the $^{27}Al/^{24}Mg$ ratios of olivine and low-Ca pyroxene are very low (typically < 0.01), the $\delta^{26}Mg^*_0$ values from isochrons and the $\delta^{26}Mg^*$ values from olivine and low-Ca pyroxene phenocrysts each represent the initial Mg isotopic compositions of chondrule-forming melts. The $\delta^{26}Mg^*_0$ (or $\delta^{26}Mg^*$) values of ferromagnesian chondrules (RF-type I and type I) are lower than $0.05‰$ and none of the data show a resolved depletion in $\delta^{26}Mg^*$ when compared to the terrestrial standards beyond analytical uncertainties (Fig. 8a). The $\delta^{26}Mg^*$ value of the Al-rich chondrule G15 is comparatively more positive, and has a relatively large uncertainty ($+0.07 \pm 0.08‰$). In addition, only low-Ca pyroxene grains were measured. Two chondrules, G45 and G48, have positive

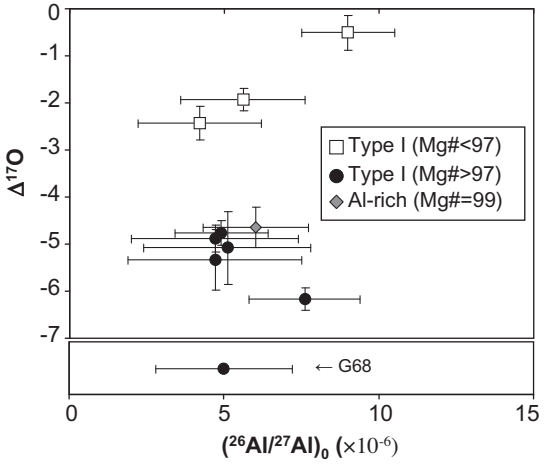

Fig. 7. Correlations between $(^{26}Al/^{27}Al)_0$ and oxygen isotopic compositions ($\Delta^{17}O$) of individual chondrules. The $(^{26}Al/^{27}Al)_0$ of the chondrule G68, which contains heterogeneity in oxygen isotope ratios (Fig. 3b) is also shown. Errors are 95% confidence.

$\delta^{26}Mg^*_0$ (or $\delta^{26}Mg^*$) values, although the observed excesses are comparable to the analytical uncertainty (2 SD) of individual analyses (Fig. 8a). As the $(^{26}Al/^{27}Al)_0$ and the $^{27}Al/^{24}Mg$ values of estimated bulk compositions of individual chondrules are distributed within a narrow range, there is no significant correlation between $\delta^{26}Mg^*_0$ (or $\delta^{26}Mg^*$) values and the $(^{26}Al/^{27}Al)_0$ or bulk $^{27}Al/^{24}Mg$ ratios of individual chondrules (Fig. 8b and c).

4.2. Mass-dependent Mg isotope fractionation

Mass-dependent fractionation of Mg isotope ratios ($\delta^{25}Mg$, ‰/amu) of olivine, pyroxene, and plagioclase of individual chondrules is summarized in Tables 2 and 3. Fig. 9 shows all $\delta^{25}Mg$ data of individual chondrules.

The observed $\delta^{25}Mg$ values of olivine and pyroxene are higher than terrestrial standards and range from 0.2‰ to 2.3‰/amu, which are consistent with results of previous studies (e.g. Galy et al., 2000; Young et al., 2002; Bizzarro et al., 2004). In most cases, olivine data contain the highest $\delta^{25}Mg$ values ($\sim +1.5$‰), followed by pyroxene ($\sim +0.6$‰), and plagioclase data have $\delta^{25}Mg$ values close to 0‰. The $\delta^{25}Mg$ values of olivine in RF-type I chondrules (G56, G100, and G113) are close to 0‰/amu, which are lower than $\delta^{25}Mg$ values of olivine in other chondrules. In the eight chondrules where both olivine and pyroxene were analyzed, $\delta^{25}Mg$ values of olivine are comparatively higher than those of pyroxene, with the exception of G74. When collectively considering the possible analytical uncertainties due to bracketing analyses of standards ($\sim \pm 0.18$‰), linear regression lines due to the matrix correction ($\sim \pm 0.15$‰), and variability in the $\delta^{25}Mg$ values of terrestrial minerals from igneous rocks ($\sim \pm 0.3$‰; Handler et al., 2009; Shen et al., 2009), the observed difference of $\delta^{25}Mg$ values (up to 1.7‰) between olivine and pyroxene within a given chondrule is significant. This result is distinct from the observation of indistinguishable oxygen isotope ratios of various phases within each chondrule (Ushikubo et al., 2012).

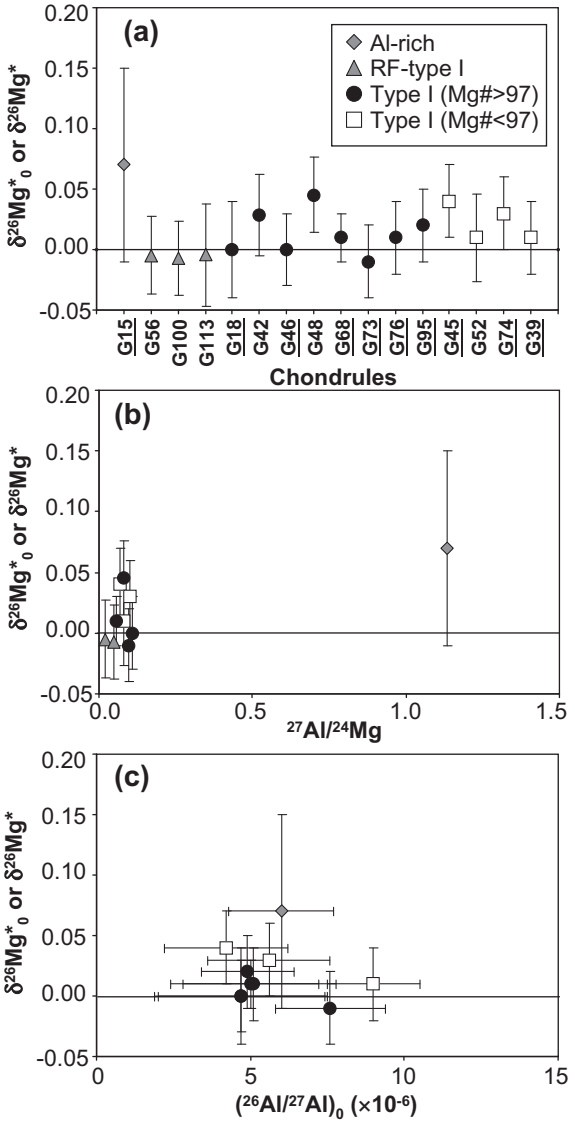

Fig. 8. (a) $\delta^{26}Mg^*_0$ or $\delta^{26}Mg^*$ values of individual chondrules. Underlined chondrule names indicate samples whose $(^{26}Al/^{27}Al)_0$ values were determined. (b) A comparison between $\delta^{26}Mg^*_0$ or $\delta^{26}Mg^*$ values and $^{27}Al/^{24}Mg$ of bulk chondrules. (c) A comparison between $\delta^{26}Mg^*_0$ or $\delta^{26}Mg^*$ values and $(^{26}Al/^{27}Al)_0$. Errors are 95% confidence.

5. DISCUSSION

5.1. Chondrule formation age and oxygen isotope systematics

5.1.1. Initial $^{26}Al/^{27}Al$ ratios and $\Delta^{17}O$ values of chondrules from Acfer 094

The range of the inferred $(^{26}Al/^{27}Al)_0$ of chondrules in Acfer 094 (Fig. 7) are similar to those from unequilibrated ordinary (LL, L) chondrites and carbonaceous (CO, CV, and Acfer 094) chondrites that typically have values of $(5–10) \times 10^{-6}$ (Hutcheon and Hutchison, 1989; Russell et al., 1996; Kita et al., 2000; Huss et al., 2001; Mostefaoui et al., 2002; Yurimoto and Wasson, 2002; Kunihiro et al., 2004; Rudraswami and Goswami, 2007; Kurahashi et al.,

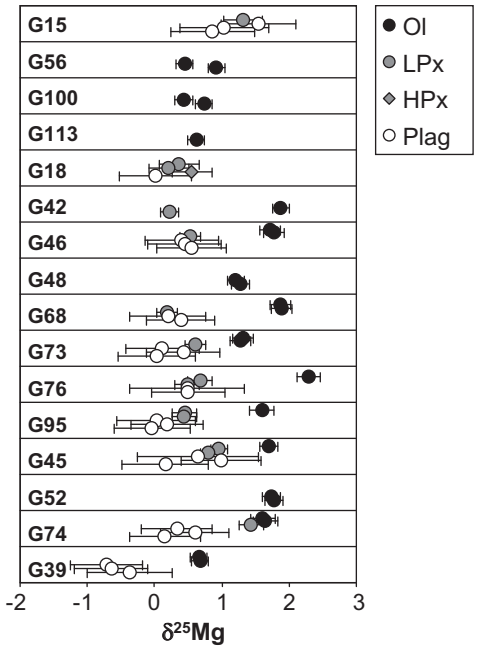

Fig. 9. δ^{25}Mg values of multiple phases of individual chondrules. The analytical uncertainty of plagioclase data is larger than those of olivine and pyroxene because of low Mg concentration in plagioclase and the usage of a lower intensity primary beam. Errors are 95% confidence level.

2008a; Rudraswami et al., 2008; Villeneuve et al., 2009; Hutcheon et al., 2009). The $(^{26}Al/^{27}Al)_0$ values in the majority of type I chondrules from Acfer 094 ($\sim 5 \times 10^{-6}$) are slightly lower than those of type I chondrules from unequilibrated ordinary and carbonaceous chondrites and are similar to those of type II chondrules from CO3 (Kunihiro et al., 2004; Kurahashi et al., 2008a). As the Mg isotopes of plagioclase and glass in chondrules from type 3.0 chondrites do not show any evidence for later isotope disturbance by metamorphism in the parent body, the ^{26}Al–^{26}Mg systematics of chondrules from type 3.0 chondrites were very likely closed after the last chondrule melting event (Kita et al., 2000; Huss et al., 2001; Kita and Ushikubo, 2012). The narrow range of $(^{26}Al/^{27}Al)_0$ values in many chondrules from Acfer 094 indicate that the last melting event occurred within a time interval of less than 0.5 Ma. Assuming a homogeneous initial distribution of extinct ^{26}Al in the early solar system (i.e., a $(^{26}Al/^{27}Al)_0$ value of 5.2×10^{-5} when primitive CAIs formed (Jacobsen et al., 2008; MacPherson et al., 2010, 2012; Larsen et al., 2011), the average $(^{26}Al/^{27}Al)_0$ value of 5.4×10^{-6} of Acfer 094 chondrules indicates that the final melting events of most chondrules from Acfer 094 occurred ~2.3 Ma after primitive CAIs.

Of this study, 14 of 16 chondrules contain internally consistent Δ^{17}O values from multiple mineral phases and glass, suggesting that the oxygen isotope ratios of chondrule-forming environments are recorded in each chondrule (Ushikubo et al., 2012). The observed increase in chondrule Δ^{17}O values associated with FeO enrichment of chondrule silicates could have been caused by enrichment of an ^{16}O-depleted oxidizing agent such as H_2O in the chondrule forming environment (Wasson et al., 2004; Connolly and Huss, 2010; Tenner et al., 2012, 2013; Ushikubo et al., 2012). This idea is supported by the proposed existence of ^{16}O-depleted H_2O in the solar nebula (Yurimoto and Kuramoto, 2004; Kuramoto and Yurimoto, 2005) and chondritic records indicating the existence of ^{16}O-depleted H_2O (Choi et al., 1998; Sakamoto et al., 2007). Interestingly, however, no significant difference in the inferred $(^{26}Al/^{27}Al)_0$ between chondrules with $\Delta^{17}O \sim -5‰$ and those with $\Delta^{17}O \sim -2‰$ is observed (Fig. 7). Two chondrules with lowest and highest Δ^{17}O values of −6.3‰ and −0.5‰, respectively, have higher inferred $(^{26}Al/^{27}Al)_0$ values of $(7–9) \times 10^{-6}$, hinting a possible change of oxygen isotope ratios with time. However, more data from chondrules with $\Delta^{17}O \sim -6‰$ and ~0‰ are necessary to determine if they consistently exhibit higher $(^{26}Al/^{27}Al)_0$ values. Overall, the narrow range of $(^{26}Al/^{27}Al)_0$ among chondrules with various Δ^{17}O values could indicate that either the oxygen isotopic composition of the solar nebula

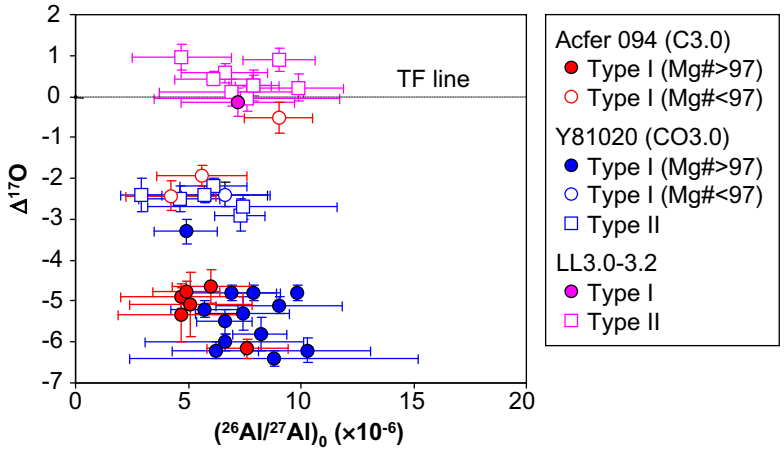

Fig. 10. A comparison of initial $^{26}Al/^{27}Al$ ratios of chondrules from Acfer 094 (C-ungrouped 3.00), Y-81020 (CO3.0), and unequilibrated ordinary chondrites (LL3.0 to 3.2) with Δ^{17}O values (data from Kita et al., 2000, 2010; Kurahashi et al., 2008a; Ushikubo et al., 2012; Tenner et al., 2013). Errors are 95% confidence.

was spatially heterogeneous, or that the increase in the abundance of an ^{16}O-depleted oxidizing agent in the chondrule forming environment occurred within the analytical uncertainty of the ^{26}Al–^{26}Mg systematics of chondrules ($\leqslant$0.3 Ma). Ushikubo et al. (2012) found that some ^{16}O-rich chondrules ($\Delta^{17}O \sim -5‰$) have ^{16}O-poor relict olivine grains ($\Delta^{17}O \sim -2‰$) and some ^{16}O-poor chondrules ($\Delta^{17}O \sim -2‰$) have ^{16}O-rich relict olivine grains ($\Delta^{17}O \sim -5‰$). This observation supports a spatial heterogeneity, rather than a temporal change, in the oxygen isotopic composition in the solar nebula.

Interestingly, the $(^{26}Al/^{27}Al)_0$ of G68, a chondrule that contains many ^{16}O-rich relict olivine grains, is consistent with those of the 14 aforementioned chondrules (Fig. 7). Although the oxygen isotope ratios of olivine in G68 suggest a close relationship to Amoeboid Olivine Aggregates (AOAs) that have ^{16}O-rich oxygen isotopic compositions and formed as early as CAIs (Hiyagon and Hashimoto, 1999; Aléon et al., 2002; Krot et al., 2005; Itoh et al., 2007; MacPherson et al., 2012), the last melting event of G68 was not older than, but instead contemporaneous to other ferromagnesian chondrules. Makide et al. (2009) reported that the compound CAI-chondrule objects have heterogeneous oxygen isotopic compositions indicating incomplete mixing between the CAI-like ^{16}O-rich component and the chondrule-like ^{16}O-poor component. The preservation of ^{16}O-rich signatures in many of the olivine grains within G68 is likely a result of incomplete melting and insufficient oxygen isotope exchange with the surrounding nebular gas.

5.1.2. Initial $^{26}Al/^{27}Al$ ratios and oxygen isotopic compositions of chondrules among primitive chondrites

Fig. 10 illustrates the comparison between $(^{26}Al/^{27}Al)_0$ and the oxygen isotopic compositions ($\Delta^{17}O$) in the same chondrules from Acfer 094, Yamato 81020 (Y-81020, CO3.0, Kurahashi et al., 2008a; Tenner et al., 2013), and three ordinary chondrites, Semarkona (LL3.0), Bishunpur (LL3.1), and Krymka (LL3.2) (Kita et al., 2000, 2010). Note that the chondrule data from a CO chondrite consist of both type I and type II chondrules but those from Acfer 094 and LL3 chondrites consist of only type I chondrules and mainly of type II chondrules, respectively.

Collectively, the chondrule data can be classified into three distinct groups with respect to their $\Delta^{17}O$ values at (1) $\geqslant$0‰, (2) $-2‰$ to $-3‰$, and (3) $<-4‰$. The first group ($\Delta^{17}O \geqslant 0‰$) mainly consists of chondrules from LL chondrites, but also contains one type I chondrule from Acfer 094 (G39). The other groups consist of chondrules from carbonaceous chondrites (Acfer 094 and Y-81020). The second group ($\Delta^{17}O = -2‰$ to $-3‰$) consist of both type I and type II chondrules, while the third group ($\Delta^{17}O < -4‰$) only consist of type I chondrules. The $(^{26}Al/^{27}Al)_0$ values of chondrules from Acfer 094 are within the ranges of those of chondrules in each of three oxygen isotope groups. Absence of chondrules with intermediate $\Delta^{17}O$ values ($-2‰$ to $-3‰$) at higher $(^{26}Al/^{27}Al)_0$ values ($\sim 1 \times 10^{-5}$, Fig. 10) suggests later formation of chondrules in oxygen isotope reservoirs of $\Delta^{17}O = -2‰$ to $-3‰$. However, there is no obvious difference in the lowest $(^{26}Al/^{27}Al)_0$ values among three oxygen isotope groups. Overall, the $(^{26}Al/^{27}Al)_0$ of all three oxygen isotope groups arguably overlap each other, meaning that there is no resolvable difference in the timing and duration of chondrule formation as a function of $\Delta^{17}O$. This indicates the presence of regional oxygen isotope heterogeneity of the solar nebula during contemporaneous formation of ordinary and carbonaceous chondrites, which was suggested by Kurahashi et al. (2008a). Although several astrophysical settings have been suggested to preserve oxygen isotope heterogeneity in the early solar nebula (e.g., Yurimoto et al., 2008), the mechanism and the source of oxygen isotope heterogeneity are not well understood.

It has been shown that majority of chondrules from CR2 chondrites have systematically lower $(^{26}Al/^{27}Al)_0$ values than those of chondrules from ordinary chondrites, Y-81020, and Acfer 094 (1×10^{-5}–4×10^{-6} for some chondrules and $<3 \times 10^{-6}$ for many chondrules, Nagashima et al., 2007, 2008; Kurahashi et al., 2008b). Oxygen isotope ratios of chondrules in CR2/CR3 chondrites have a wide range of $\Delta^{17}O$ values ($-5‰$ to $+1‰$; Connolly and Huss, 2010; Tenner et al., 2012; Schrader et al., 2013), though there is no systematic study that combines their ^{26}Al–^{26}Mg systematics with oxygen isotope ratios. A $\Delta^{17}O \sim 0‰$ chondrule fragment from the Jupiter-family comet Wild 2 also has lower $(^{26}Al/^{27}Al)_0$ ($<3.0 \times 10^{-6}$; Ogliore et al., 2012). Collectively, these chondrules could represent a younger generation of chondrules that formed in regionally heterogeneous oxygen isotope composition of the solar nebula.

5.2. Magnesium isotopic composition of chondrules

5.2.1. Mass-dependent fractionation

Olivine grains in chondrules have variable and positively fractionated Mg isotopic compositions (up to 2.3‰ in δ^{25}Mg, Fig. 9). In contrast, Mg isotopic compositions of low-Ca pyroxene and plagioclase in the same chondrules tend to show less fractionation, with the exception of low-Ca pyroxene in the chondrule G74 (Fig. 9). The occurrence of a positive Mg isotopic fractionation in Allende chondrule olivine has also been suggested by Villeneuve et al. (2011). As equilibrium Mg isotope fractionation ($^{26}Mg/^{24}Mg$) between olivine and melt is less than 0.07‰ at $\geqslant$1055 °C (Teng et al., 2007), the observed variation of δ^{25}Mg in each chondrule indicates that Mg isotopes were fractionated by evaporation and/or condensation during chondrule melting processes.

Although it has been recognized that the degree of mass-dependent isotope fractionation of various elements such as K, Mg, and Fe in chondrules is limited and significantly smaller than those by Rayleigh-type evaporative loss (e.g. Galy et al., 2000; Alexander and Wang, 2001; Alexander and Grossman, 2005; Hezel et al., 2010), it has been suggested that isotopic compositions of chondrule-forming melt were initially positively fractionated because of evaporative loss at the beginning of chondrule formation, and that the signature of mass fractionation was erased by later condensation of elements from the surrounding gas (e.g., Alexander, 2004; Fedkin et al., 2012). If type I chondrules

formed in a less dust-enriched environment than type II chondrules (e.g., Ebel and Grossman, 2000; Alexander, 2004), the temporal positive isotopic fractionation during chondrule formation is more likely to occur for type I chondrule melts although the degree of isotopic fractionation highly depends on the conditions of chondrule formation. Furthermore, Nagahara et al. (2008) reported evidence for condensation of Mg and Si at the cooling stage of chondrule formation. Therefore, it is possible that the systematically higher δ^{25}Mg values in olivine observed from many type I chondrules from Acfer 094 could represent temporal enrichments of heavy Mg isotopes, due to evaporative effects during high temperature crystallization of olivine from the chondrule-forming melt. Pyroxene and plagioclase likely crystallized after olivine, and possibly after recondensation and incorporation of Mg into the chondrule-forming melt, so that they acquired progressively lower δ^{25}Mg values relative to olivine.

The lack of a systematic correlation in oxygen isotopes could mean that (1) the mass-dependent fractionation of oxygen isotopes by evaporative loss was smaller than that of Mg isotopes (e.g. Wang et al., 2001) and the analytical uncertainties of δ^{18}O values for ferromagnesian silicates and plagioclase (±0.3‰ and ±1.2‰, respectively; Ushikubo et al., 2012) are insufficient to distinguish a variation in δ^{18}O values or (2) the interaction and re-equilibration between melt and surrounding gas during chondrule formation (e.g. Alexander, 2004) might have suppressed mass-dependent isotope fractionation. Due to the relatively small chondrule sizes in Acfer 094, detailed study on internal variations of δ^{25}Mg and a comparison between Mg and oxygen isotope ratios within a chondrule could not be examined in this study. Perhaps future investigations of δ^{25}Mg variations within chondrule phases, likely within larger chondrules (e.g. chondrules from LL, CV, CR chondrites), will prove useful in addressing temporal isotope fractionation during chondrule formation.

We obtained one Mg isotope measurement from a relict olivine grain (G68 ol#1, Fig. 1d) which exhibits a highly ^{16}O-rich oxygen isotope ratio ($\Delta^{17}O \sim -18‰$, Fig. 3b, Table 2). Even though the oxygen isotope ratio of this olivine grain is similar to those of AOAs, the Mg isotope ratio is positively fractionated. This observation is distinct from a lack of positive Mg isotope fractionation in AOAs (e.g., MacPherson et al., 2012) but is similar to olivine grains in chondrules whose oxygen isotope ratios are homogeneous. The relict grain is coarser (~60 μm in diameter) than those of AOAs and its oxygen isotope ratio is not as ^{16}O-rich as typical AOAs (e.g., Krot et al., 2004). One possible explanation is that we measured a mixture of relict and overgrowth within the single olivine grain. Another possibility is that both oxygen and Mg isotopes of this grain were partially disturbed by annealing and isotopic diffusion during the chondrule melting process.

5.2.2. $\delta^{26}Mg^*$ variations in chondrules

Three olivine data from three chondrules (G45, G48, and G74) exhibit positive $\delta^{26}Mg^*$. However, their values are within the 3SE errors of individual analyses. No negative $\delta^{26}Mg^*$ was observed, including the analysis of the ^{16}O-rich ($\Delta^{17}O \sim -18‰$) olivine grain within chondrule G68 (spot #1 in Table 2). Although olivine grains with an ^{16}O-rich signature are as old as CAIs, an expected $\delta^{26}Mg^*$ should only be as low as −0.03‰ (Jacobsen et al., 2008; Villeneuve et al., 2009), which is smaller than a typical uncertainty of each analysis in this study (±0.05‰). We could not perform multiple Mg isotope analyses in each olivine grain to confirm subtle $\delta^{26}Mg^*$ variation because the primary beam size is comparable to the size of each measured grain. Further data are required to confirm the existence of $\delta^{26}Mg^*$ variability in olivine.

In contrast, two low-Ca pyroxene data in two type IAB chondrules, G45 and G74, exhibit positive $\delta^{26}Mg^*$ values of ~0.13‰, which are significantly higher than the 3SE of low-Ca pyroxene analysis and ~0.1‰ higher than other coexisting olivine and pyroxene grains within the same chondrule (Table 2). Considering the inferred $(^{26}Al/^{27}Al)_0$ of these chondrules (~5.4×10^{-6}) and low $^{27}Al/^{24}Mg$ ratios of their constituent low-Ca pyroxene grains (<0.11), the values of these unique, high $\delta^{26}Mg^*$ grains are much larger than expected (<0.005‰). It is unlikely that low-Ca pyroxene preserved an intrinsic positive $\delta^{26}Mg^*$ of precursor silicate dust because oxygen isotope ratios indicate that low-Ca pyroxene crystallized from the chondrule forming melt (Ushikubo et al., 2012). A possible explanation is that these pyroxene grains formed by reheating and partial melting of chondrules. If a chondrule was reheated and partially melted, the melt could have a higher Al/Mg ratio than that of the bulk chondrule because of presence of unmelted ferromagnesian silicates (e.g., olivine). If the radiogenic ^{26}Mg accumulated in previous Al-rich phases was redistributed in the melt, then any phases, including pyroxene, plagioclase, and glass, formed from the melt would have an excess in ^{26}Mg relative to the other crystalline phases from the earlier chondrule forming event. If so, the pyroxene data with elevated $\delta^{26}Mg^*$ may represent direct evidence for a repeated melting of chondrules. In such a scenario, the inferred $(^{26}Al/^{27}Al)_0$ by the isochron from plagioclase and pyroxene with excess ^{26}Mg represents the ^{26}Al abundance when such a partial melting occurred. Multiple heating events of chondrules may have occurred with a time scale comparable to the observed variations in ^{26}Al relative ages within a single meteorite group, typically 0.5–1 Ma (e.g., Kita and Ushikubo, 2012).

By alternatively using these pyroxene grains with higher $\delta^{26}Mg^*$ as initial Mg isotope ratios, the inferred $(^{26}Al/^{27}Al)_0$ values would be slightly lower than those shown in Fig. 6; $(4.0 \pm 2.0) \times 10^{-6}$ for G45 and $(5.3 \pm 2.0) \times 10^{-6}$ for G74, respectively. These alternate values do not change the slopes of isochron regression significantly because plagioclase grains have high $^{27}Al/^{24}Mg$ ratios ($\geqslant 30$) and their $\delta^{26}Mg^*$ values of plagioclase ($\geqslant 1‰$) are significantly higher than those of high $\delta^{26}Mg^*$ pyroxene grains. If an isochron of chondrules only be determined using lower $^{27}Al/^{24}Mg$ phases (e.g., Al-rich glass with $^{27}Al/^{24}Mg < 10$), these differences in pyroxene analyses would yield a greater uncertainty in the slope of the isochron. Therefore, careful analysis of pyroxene would be required to assess the inferred $(^{26}Al/^{27}Al)_0$ of chondrules.

6. CONCLUSIONS

We determined $(^{26}Al/^{27}Al)_0$ of one Al-rich chondrule and 9 type I chondrules from the Acfer 094 carbonaceous chondrite (C-ungrouped 3.00) and compared these values with corresponding chondrule oxygen isotope ratios. We also measured Mg isotopic compositions of 3 type I and 3 RF-type I chondrules that have been previously measured for their oxygen isotope ratios.

1. Although significant variability is observed in $(^{26}Al/^{27}Al)_0$ of Acfer 094 chondrules, no strong correlation exists between $(^{26}Al/^{27}Al)_0$ and $\Delta^{17}O$ values. This is true even when chondrules from Y-81020 (CO3.0) and unequilibrated ordinary chondrites (LL3.0 to 3.2) are included, indicating regional oxygen isotope heterogeneity in the solar nebula over the duration of chondrule formation.
2. The ^{26}Al–^{26}Mg systematics of the type I chondrule G68, which has olivine grains with highly heterogeneous oxygen isotope ratios (down to $-23‰$ in $\Delta^{17}O$), indicates that the timing of the last melting of this chondrule was similar to other ferromagnesian chondrules. The ^{16}O-rich signature of this chondrule suggests that the precursor material was closely related to refractory inclusions. However, preservation of the ^{16}O-rich signature is not the result of an earlier stoppage of the last chondrule melting process, but is likely rather the result of incomplete melting and insufficient oxygen isotope exchange with the surrounding nebular gas during chondrule melting.
3. Magnesium isotopes of olivine grains of chondrules are positively fractionated. As olivine is the liquidus phase in the chondrules investigated in this study, it may preserve a positively fractionated Mg isotopic composition of the chondrule forming melt prior to significant condensation of major elements that occurred during the cooling stage of chondrule formation.
4. A positive $\delta^{26}Mg^*$ was observed in a few low-Ca pyroxene grains, with $\delta^{26}Mg^*$ values that are $\sim 0.1‰$ greater than other coexisting olivine and pyroxene grains within the same chondrule. This may be the result of a partial melting of chondrules by a reheating event, by which the high $\delta^{26}Mg^*$ low-Ca pyroxene crystallized and exchanged Mg isotopes. If this is the case, the true $(^{26}Al/^{27}Al)_0$ of the last chondrule melting event of some chondrules would be slightly lower (by $<10\%$) than the $(^{26}Al/^{27}Al)_0$ based on Mg isotope data of plagioclase and olivine.

ACKNOWLEDGEMENTS

The authors thank Glenn J. MacPherson and Linda Welzenbach, Smithsonian Institute, for the use of Acfer 094 thin section. Harold C. Connolly J.r, Hisayoshi Yurimoto, and Kazuhide Nagashima provided helpful comments that improved this manuscript. This work is supported by NASA (NNX07AI46G, NNX11AG62G, NK) and a Grant-in-aids of Ministry of Education, Science, and Culture (No. 22540488, MK). WiscSIMS is partly supported by NSF (EAR03-19230, EAR07-44079).

APPENDIX A. SUPPLEMENTARY DATA

Supplementary data associated with this article can be found, in the online version, at http://dx.doi.org/10.1016/j.gca.2013.01.045.

REFERENCES

Aléon J., Krot A. N. and McKeegan K. D. (2002) Calcium–aluminum-rich inclusions and amoeboid olivine aggregates from the CR carbonaceous chondrites. *Meteorit. Planet. Sci.* **37**, 1729–1755.

Alexander C. M. O'D. (2004) Chemical equilibrium and kinetic constraints for chondrule and CAI formation conditions. *Geochim. Cosmochim. Acta* **68**, 3943–3969.

Alexander C. M. O'D. and Wang J. (2001) Iron isotopes in chondrules: implications for the role of evaporation during chondrule formation. *Meteorit. Planet. Sci.* **36**, 419–428.

Alexander C. M. O'D. and Grossman J. N. (2005) Alkali elemental and potassium isotopic compositions of Semarkona chondrules. *Meteorit. Planet. Sci.* **40**, 541–556.

Amelin Y., Krot A. N., Hutcheon I. D. and Ulyanov A. A. (2002) Lead isotopic ages of chondrules and calcium–aluminum-rich inclusions. *Science* **297**, 1678–1683.

Amelin Y., Kaltenbach A., Iizuka T., Stirling C. H., Ireland T. R., Petaev M. and Jacobsen S. B. (2010) U–Pb chronology of the solar system's oldest solids with variable $^{238}U/^{235}U$. *Earth Planet. Sci. Lett.* **300**, 343–350.

Bizzarro M., Baker J. A. and Haack H. (2004) Mg isotope evidence for contemporaneous formation of chondrules and refractory inclusions. *Nature* **431**, 275–278.

Catanzaro E. J., Murphy T. J., Garner E. L. and Shields W. R. (1966) Absolute isotopic abundance ratios and atomic weights of magnesium. *J. Res. Natl. Bur. Stand.* **70a**, 453–458.

Choi B.-G., McKeegan K. D., Krot A. N. and Wasson J. T. (1998) Extreme oxygen-isotope compositions in magnetite from unequilibrated ordinary chondrites. *Nature* **392**, 577–579.

Connelly J. N., Amelin Y., Krot A. N. and Bizzarro M. (2008) Chronology of the solar system's oldest solids. *Astrophys. J.* **675**, L121–L124.

Connolly, Jr., H. C. and Huss G. R. (2010) Compositional evolution of the protoplanetary disk: oxygen isotopes of type-II chondrules from CR2 chondrites. *Geochim. Cosmochim. Acta* **74**, 2473–2483.

Connolly, Jr., H. C. and Love S. G. (1998) The formation of chondrules: petrologic tests of the shock wave model. *Science* **280**, 62–67.

Davis A. M., Richter F. M., Mendybaev R. A., Janney P. E., Wahdwa M. and McKeegan K. D. (2005) Isotopic mass fractionation laws and the initial Solar System 26Al/27Al ratio. *36th Lunar Planetary Science Conference*, CD-ROM (abstr. #2334).

Ebel D. S. and Grossman L. (2000) Condensation in dust-enriched systems. *Geochim. Cosmochim. Acta* **64**, 339–366.

Fedkin A. V., Grossman L., Ciesla F. J. and Simon S. B. (2012) Mineralogical and isotopic constraints on chondrule formation from shock wave thermal histories. *Geochim. Cosmochim. Acta* **87**, 81–116.

Fedkin A. V. and Grossman L. (2006) The fayalite content of chondritic olivine: obstacle to understanding the condition of rocky material. In *Meteorites and the Early Solar System II* (eds. D. S. Lauretta and H. Y. McSween Jr.). The University of Arizona Press, Tucson, AZ, pp. 279–294.

Galy A., Young E. D., Ash R. D. and O'Nions R. K. (2000) The formation of chondrules at high gas pressures in the solar nebula. *Nature* **290**, 1751–1753.

Greshake A. (1997) The primitive matrix components of the unique carbonaceous chondrite Acfer 094: a TEM study. *Geochim. Cosmochim. Acta* **61**, 437–452.

Grossman J. N. and Brearley A. J. (2005) The onset of metamorphism in ordinary and carbonaceous chondrites. *Meteorit. Planet. Sci.* **40**, 87–122.

Handler M. R., Baker J. A., Schiller M., Bennett V. C. and Yaxley G. M. (2009) Magnesium stable isotope composition of Earth's upper mantle. *Earth Planet. Sci. Lett.* **282**, 306–313.

Hezel D. C., Needham A. W., Armytage R., Georg B., Abel R. L., Kurahashi E., Coles B. J., Rehkämper M. and Russell S. S. (2010) A nebular setting as the origin for bulk chondrule Fe isotope variations in CV chondrites. *Earth Planet. Sci. Lett.* **296**, 423–433.

Hiyagon H. and Hashimoto A. (1999) ^{16}O excesses in olivine inclusions in Yamato-86009 and Murchison chondrites and their relation to CAIs. *Science* **283**, 828–831.

Huss G. R., MacPherson G. J., Wasserburg G. J., Russell S. S. and Srinivasan G. (2001) Aluminum-26 in calcium–aluminum-rich inclusions and chondrules from unequilibrated ordinary chondrites. *Meteorit. Planet. Sci.* **36**, 975–997.

Hutcheon I. D. and Hutchison R. (1989) Evidence from the Semarkona ordinary chondrite for ^{26}Al heating of small planets. *Nature* **337**, 238–241.

Hutcheon I. D., Marhas K. K., Krot A. N., Goswami J. N. and Jones R. H. (2009) ^{26}Al in plagioclase-rich chondrules in carbonaceous chondrites: evidence for an extended duration of chondrule formation. *Geochim. Cosmochim. Acta* **73**, 5080–5099.

Ikeda Y. (1980) Petrology of Allan Hills-764 chondrite (LL3). *Mem. Natl. Inst. Polar Res. Spec.* **17**, 50–82.

Itoh S., Russell S. S. and Yurimoto H. (2007) Oxygen and magnesium isotopic compositions of amoeboid olivine aggregates from the Semarkona LL3.0 chondrite. *Meteorit. Planet. Sci.* **42**, 1241–1247.

Jacobsen B., Yin Q.-Z., Moynier F., Amelin Y., Krot A. N., Nagashima K., Hutcheon I. D. and Palme H. (2008) ^{26}Al–^{26}Mg and ^{207}Pb–^{206}Pb systematics of Allende CAIs: canonical solar initial $^{26}Al/^{27}Al$ ratio reinstated. *Earth Planet. Sci. Lett.* **272**, 353–364.

Kimura M., Grossman J. N. and Weisberg M. K. (2008) Fe–Ni metal in primitive chondrites: indicators of classification and metamorphic conditions for ordinary and CO chondrites. *Meteorit. Planet. Sci.* **43**, 1161–1177.

Kita N. T., Nagahara H., Tachibana S., Tomomura S., Spicuzza M. J., Fournelle J. H. and Valley J. W. (2010) High precision SIMS oxygen three isotope study of chondrules in LL3 chondrites: role of ambient gas during chondrule formation. *Geochim. Cosmochim. Acta* **74**, 6610–6635.

Kita N. T., Nagahara H., Togashi S. and Morishita Y. (2000) A short duration of chondrule formation in the solar nebula: evidence from ^{26}Al in Semarkona ferromagnesian chondrules. *Geochim. Cosmochim. Acta* **64**, 3913–3922.

Kita N. T. and Ushikubo T. (2012) Evolution of protoplanetary disk inferred from ^{26}Al chronology of individual chondrules. *Meteorit. Planet. Sci.* **47**, 1108–1119.

Kita N. T., Ushikubo T., Knight K. B., Mendybaev R. A., Davis A. M., Richter F. M. and Fournelle J. H. (2012) Internal ^{26}Al–^{26}Mg isotope systematics of a type B CAI: remelting of refractory precursor solids. *Geochim. Cosmochim. Acta* **86**, 37–51.

Krot A. N., Fagan T. J., Nagashima K., Petaev M. I. and Yurimoto H. (2005) Origin of low-Ca pyroxene in amoeboid olivine aggregates: evidence from oxygen isotopic compositions. *Geochim. Cosmochim. Acta* **69**, 1873–1881.

Krot A. N., Petaev M. I., Russell S. S., Itoh S., Fagan T. J., Yurimoto H., Chizmadia L., Weisberg M. K., Komatsu M., Ulyanov A. A. and Keil K. (2004) Amoeboid olivine aggregates and related objects in carbonaceous chondrites: records of nebular and asteroid processes. *Chem. Erde* **64**, 185–239.

Kunihiro T., Rubin A. E., McKeegan K. D. and Wasson J. T. (2004) Initial $^{26}Al/^{27}Al$ in carbonaceous-chondrite chondrules: too little ^{26}Al to melt asteroids. *Geochim. Cosmochim. Acta* **68**, 2947–2957.

Kurahashi E., Kita N. T., Nagahara H. and Morishita Y. (2008a) ^{26}Al–^{26}Mg systematics of chondrules in a primitive CO chondrite. *Geochim. Cosmochim. Acta* **72**, 3865–3882.

Kurahashi E., Kita N. T., Nagahara H. and Morishita Y. (2008b) ^{26}Al–^{26}Mg systematics and petrological study of chondrules in CR chondrites. *Geochim. Cosmochim. Acta* **72**, A504 (abstr.).

Kuramoto K. and Yurimoto H. (2005) Oxygen isotopic heterogeneity in the solar system: the molecular cloud origin hypothesis and its implications for meteorites and the planets. In *Astronomical Society of the Pacific Conference Series. Chondrites and the Protoplanetary Disk*, vol. 341 (eds. A. N. Krot, E. R. Scott and B. Reipurth). Astronomical Society of the Pacific, San Francisco, CA, pp. 181–192.

Larsen K. K., Triquier A., Paton C., Schiller M., Wielandt D., Ivanova M. A., Connelly J. N., Nordlund Å., Krot A. N. and Bizzarro M. (2011) Evidence for magnesium isotope heterogeneity in the solar protoplanetary disk. *Astrophys. J. Lett.* **735**, L37.

MacPherson G. J., Bullock E. S., Janney P. E., Kita N. T., Ushikubo T., Davis A. M., Wahdwa M. and Krot A. N. (2010) Early solar nebula condensates with canonical, not supracanonical, initial $^{26}Al/^{27}Al$ ratios. *Astrophys. J. Lett.* **711**, L117–L121.

MacPherson G. J., Kita N. T., Ushikubo T., Bullock E. S. and Davis A. M. (2012) Well-resolved variations in the formation ages for Ca–Al-rich inclusions in the early solar system. *Earth Planet. Sci. Lett.* **331–332**, 43–54.

Makide K., Nagashima K., Krot A. N., Huss G. R., Hutcheon I. D. and Bischoff A. (2009) Oxygen- and magnesium-isotope compositions of calcium–aluminum-rich inclusions from CR2 carbonaceous chondrites. *Geochim. Cosmochim. Acta* **73**, 5018–5050.

Mostefaoui S., Kita N. T., Togashi S., Tachibana S., Nagahara H. and Morishita Y. (2002) The relative formation ages of ferromagnesian chondrules inferred from their initial aluminum-26/aluminum-27 ratios. *Meteorit. Planet. Sci.* **37**, 421–438.

Nagahara H., Kita N. T., Ozawa K. and Morishita Y. (2008) Condensation of major elements during chondrule formation and its implication to the origin of chondrules. *Geochim. Cosmochim. Acta* **72**, 1442–1465.

Nagashima K., Krot A. N. and Chaussidon M. (2007) Aluminum–magnesium isotope systematics of chondrules from CR chondrites. *Meteorit. Planet. Sci. Suppl.* **42**, 5291 (abstr.).

Nagashima K., Krot A. N. and Huss G. (2008) 26Al in chondrules from CR carbonaceous chondrites. *39th Lunar Planetary Science Conference*, CD-ROM (abstr. #2224).

Nakashima D., Kimura M., Yamada K., Noguchi T., Ushikubo T. and Kita N. T. (2010) Study of chondrules in CH chondrites – I: oxygen isotope ratios of chondrules. *Meteorit. Planet. Sci. Suppl.* **45**, A148 (abstr.).

Norris T. L., Gancarz A. J., Rokop D. J. and Thomas K. W. (1983) Half-life of ^{26}Al. *J. Geophys. Res.* **88**, B331–B333.

Ogliore R. C., Huss G. R., Nagashima K., Butterworth A. L., Gainsforth Z., Stodolna J., Westphal A. J., Joswiak D. and Tyliszczak T. (2012) Incorporation of a late-forming chondrule into comet Wild 2. *Astrophys. J. Lett.* **745**, L19.

Rudraswami N. G. and Goswami J. N. (2007) ^{26}Al in chondrules from unequilibrated L chondrites: onset and duration of chondrule formation in the early solar system. *Earth Planet. Sci. Lett.* **257**, 231–244.

Rudraswami N. G., Goswami J. N., Chattopadhyay B., Sengupta S. K. and Thapliyal A. P. (2008) ^{26}Al records in chondrules from unequilibrated ordinary chondrites: II. Duration of chondrule formation and parent body thermal metamorphism. *Earth Planet. Sci. Lett.* **274**, 93–102.

Rudraswami N. G., Ushikubo T., Nakashima D. and Kita N. T. (2011) Oxygen isotope systematics of chondrules in Allende CV3 chondrite: high precision ion microprobe studies. *Geochim. Cosmochim. Acta* **75**, 7596–7611.

Russell S. S., Srinivasan G., Huss G. R., Wasserburg G. J. and MacPherson G. J. (1996) Evidence for widespread ^{26}Al in the solar nebula and constraints for nebula time scale. *Science* **273**, 757–762.

Sakamoto N., Seto Y., Itoh S., Kuramoto K., Fujino K., Nagashima K., Krot A. N. and Yurimoto H. (2007) Remnants of the early solar system water enriched in heavy oxygen isotopes. *Science* **317**, 231–233.

Schrader D. L., Connolly, Jr., H. C., Lauretta D. S., Nagashima K., Huss G. R., Davidson J. and Domanik K. J. (2013) The formation and alteration of the Renazzo-like carbonaceous chondrites II: linking O-isotope composition and oxidation state of chondrule olivine. *Geochim. Cosmochim. Acta* **101**, 302–327.

Shen B., Jacobsen B., Lee C.-T. A., Yin Q.-Z. and Morton D. M. (2009) The Mg isotopic systematics of granitoids in continental arcs and implications for the role of chemical weathering in crust formation. *Proc. Natl. Acad. Sci.* **106**, 20652–20657.

Steele I. M. (1986) Compositions and textures of relic forsterite in carbonaceous and unequilibrated ordinary chondrites. *Geochim. Cosmochim. Acta* **50**, 1379–1395.

Teng F.-Z., Wahdwa M. and Helz R. T. (2007) Investigation of magnesium isotope fractionation during basalt differentiation: implications for a chondritic composition of the terrestrial mantle. *Earth Planet. Sci. Lett.* **261**, 84–92.

Teng F.-Z., Li W.-Y., Ke S., Marty B., Dauphas N., Huang S., Wu F.-Y. and Pourmand A. (2010) Magnesium isotopic composition of the Earth and chondrites. *Geochim. Cosmochim. Acta* **74**, 4150–4166.

Tenner T. J., Nakashima D., Ushikubo T., Kita N. T. and Weisberg M. K. (2012) Oxygen isotopes of chondrules in the Queen Alexandra Range 89177 CR3 chondrite: Further evidence for systematic relationships between chondrule Mg# and Δ^{17}O and the role of ice during chondrule formation. *43rd Lunar Planetary Science Conference*, CD-ROM (abstr. #1659).

Tenner T. J., Ushikubo T., Kurahashi E., Kita N. T. and Nagahara H. (2013) Oxygen isotope systematics of chondrule phenocrysts from the CO3.0 chondrite Yamato 81020: evidence for two distinct oxygen isotope reservoirs. *Geochim. Cosmochim. Acta* **102**, 226–245.

Ushikubo T., Kimura M., Kita N. T. and Valley J. W. (2012) Primordial oxygen isotope reservoirs of the solar nebula recorded in chondrules. *Geochim. Cosmochim. Acta* **90**, 242–264.

Van Orman J. A., Cherniak D. J. and Kita N. T. (2012) Magnesium diffusion in plagioclase. *43rd Lunar Planetary Science Conference*, CD-ROM (abstr. #1467).

Villeneuve J., Chaussidon M. and Libourel G. (2009) Homogeneous distribution of ^{26}Al in the solar system from the Mg isotopic composition of chondrules. *Science* **325**, 985–988.

Villeneuve J., Chaussidon M. and Libourel G. (2011) Magnesium isotopes constraints on the origin of Mg-rich olivines from the Allende chondrite: nebular versus planetary? *Earth Planet. Sci. Lett.* **301**, 107–116.

Wang J., Davis A. M., Clayton R. N., Mayeda T. and Hashimoto A. (2001) Chemical and isotopic fractionation during the evaporation of the FeO–MgO–SiO_2–CaO–Al_2O_3–TiO_2 rare earth element melt system. *Geochim. Cosmochim. Acta* **65**, 479–494.

Wasson J. T., Rubin A. E. and Yurimoto H. (2004) Evidence in CO3.0 chondrules fro a drift in the O isotopic composition of the solar nebula. *Meteorit. Planet. Sci.* **39**, 1591–1598.

Young E. D., Ash R. D., Galy A. and Belshaw N. S. (2002) Mg isotope heterogeneity in the Allende meteorite measured by UV laser ablation-MC-ICPMS and comparisons with O isotopes. *Geochim. Cosmochim. Acta* **66**, 683–698.

Yurimoto H., Krot A. N., Choi B.-G., Aléon J., Kunihiro T. and Brearley A. J. (2008) Oxygen isotopes of chondritic components. In *Reviews in Mineralogy & Geochemistry 68 Oxygen in the Solar System* (eds. G. J. MacPherson, D. W. Mittlefehldt, J. H. Johnes, S. B. Simon, J. J. Papike and S. Mackwell). Mineralogical Society of America, Chantilly, VA, pp. 141–186.

Yurimoto H. and Kuramoto K. (2004) Molecular cloud origin for the oxygen isotope heterogeneity in the solar system. *Science* **305**, 1763–1766.

Yurimoto H. and Wasson J. T. (2002) Extremely rapid cooling of a carbonaceous-chondrite chondrule containing very ^{16}O-rich olivine and a ^{26}Mg-excess. *Geochim. Cosmochim. Acta* **66**, 4355–4363.

Associate editor: Yuri Amelin